

HCN1 Channels Constrain Synaptically Evoked Ca^{2+} Spikes in Distal Dendrites of CA1 Pyramidal Neurons

David Tsay,¹ Joshua T. Dudman,¹ and Steven A. Siegelbaum^{1,2,3,*}

¹Department of Neuroscience

²Department of Pharmacology

³Howard Hughes Medical Institute

Columbia University, 1051 Riverside Drive, New York, NY 10032, USA

*Correspondence: sas8@columbia.edu

DOI 10.1016/j.neuron.2007.11.015

SUMMARY

HCN1 hyperpolarization-activated cation channels act as an inhibitory constraint of both spatial learning and synaptic integration and long-term plasticity in the distal dendrites of hippocampal CA1 pyramidal neurons. However, as HCN1 channels provide an excitatory current, the mechanism of their inhibitory action remains unclear. Here we report that HCN1 channels also constrain CA1 distal dendritic Ca^{2+} spikes, which have been implicated in the induction of LTP at distal excitatory synapses. Our experimental and computational results indicate that HCN1 channels provide both an active shunt conductance that decreases the temporal integration of distal EPSPs and a tonic depolarizing current that increases resting inactivation of T-type and N-type voltage-gated Ca^{2+} channels, which contribute to the Ca^{2+} spikes. This dual mechanism may provide a general means by which HCN channels regulate dendritic excitability.

INTRODUCTION

Hippocampal activity-dependent long-term synaptic plasticity is widely thought to be a key cellular substrate for spatial learning and memory (Morris et al., 2003). Due to the cooperative and associative nature of such forms of plasticity, the individual postsynaptic potentials from a large number of synaptic inputs must be integrated by neuronal dendrites to elicit a postsynaptic response sufficient to induce plastic changes. Over the past several years it has become clear that dendrites are endowed with a wide array of voltage-gated ion channels that shape the integration of synaptic inputs and enable the active processing of synaptic information (London and Hausser, 2005; Magee and Johnston, 2005). Although much is now known about the molecular mechanisms underlying

synaptic plasticity, we understand less about how the active integrative properties of neuronal dendrites influence the induction of synaptic plasticity to regulate learning and memory.

Here we focus on the role of the hyperpolarization-activated cation current (I_h), encoded by the HCN channel gene family (*HCN1-4*; Robinson and Siegelbaum, 2003), in the regulation of dendritic excitability and long-term synaptic plasticity in hippocampal CA1 pyramidal neurons. HCN1 is highly expressed in the apical dendrites of the CA1 neurons in a gradient of increasing density with increasing distance from the soma (Lorincz et al., 2002; Magee, 1998; Notomi and Shigemoto, 2004; Santoro et al., 2000). Mice with a forebrain-restricted deletion of HCN1 show an increase in spatial learning and an increase in temporal integration and long-term potentiation (LTP) of EPSPs generated at the perforant path (PP) inputs to the CA1 neurons (Nolan et al., 2004). These inputs, which arise from layer 3 neurons of entorhinal cortex, terminate on the distal CA1 dendrites in stratum lacunosum moleculare (SLM), the site of greatest HCN1 channel density. Thus, HCN1 channels exert an inhibitory constraint on dendritic integration and synaptic plasticity at the PP inputs to CA1 pyramidal neurons and constrain hippocampal-dependent spatial learning.

The inhibitory effect of HCN1 revealed by its genetic deletion is consistent with previous studies on the role of I_h in dendritic integration. Application of the organic I_h antagonist ZD7288 enhances the magnitude of the voltage change during an EPSP and slows the time course of EPSP decay, increasing temporal integration in both CA1 pyramidal neurons (Magee, 1998, 1999) and neocortical layer 5 pyramidal cells (Stuart and Spruston, 1998; Williams and Stuart, 2000; Berger et al., 2003). Blockade of I_h also facilitates the firing of local spikes in CA1 dendrites in stratum radiatum (Magee, 1999; Poolos et al., 2002) and lowers the threshold for the activation of dendritic Ca^{2+} spikes triggered by backpropagating action potentials in layer 5 neurons (Berger et al., 2003). Conversely, upregulation of I_h in CA1 neurons by the anticonvulsant lamotrigine (Poolos et al., 2002) and in entorhinal

cortex neurons by dopamine (Rosenkranz and Johnston, 2006) inhibits firing of dendritic action potentials.

Previous studies have ascribed the inhibitory actions of I_h to its being partially active at the resting potential, providing a shunt conductance that decreases input resistance, membrane time constant, and temporal integration, which decreases the depolarization during an EPSP (Magee, 1998; Stuart and Spruston, 1998; Poolos et al., 2002). However, since the I_h reversal potential (~ -30 mV) is positive to the threshold for spike firing (-50 to -40 mV), I_h generates an excitatory current at subthreshold voltages. As a result, blockade of I_h hyperpolarizes the resting membrane by 5–10 mV, which counteracts any increase in the magnitude of a subthreshold EPSP due to the increase in input resistance. In a simple model containing only I_h , a leak conductance, and an excitatory synaptic input, the absolute peak EPSP voltage is actually closer to threshold in the presence of I_h than in its absence. Indeed, the excitatory effect of I_h underlies its contribution to spontaneous rhythmic firing in both the heart and in central neurons (Robinson and Siegelbaum, 2003). Thus, despite the general finding that I_h exerts a potent inhibitory control on dendritic excitability, the mechanism underlying this inhibitory action and its constraint on the induction of LTP remains unclear.

In this study we have investigated the possibility that HCN channels produce their inhibitory effects on synaptic plasticity by nonlinear interactions with other dendritic voltage-gated channels. In particular, we have used Ca²⁺ imaging to investigate the effects of I_h on local regenerative calcium spikes in CA1 neuron distal dendrites (Golding et al., 2002; Wei et al., 2001), as such spikes have been suggested to be important for the induction of PP LTP (Golding et al., 2002). We find that either genetic deletion of HCN1 or pharmacological blockade of I_h enhances the amplitude and duration of distal nonlinear dendritic Ca²⁺ events evoked by a brief tetanic burst of perforant path synaptic stimulation. Our computational and experimental data indicate that this effect is due to the combined action of the reduction in I_h to hyperpolarize the membrane and enhance dendritic integration through an increase in input resistance. The hyperpolarization reduces resting inactivation of T-type and N-type voltage-gated calcium channels (VGCCs), which contribute to Ca²⁺ influx during the dendritic spikes; the increase in input resistance increases the amplitude of the EPSP, helping to offset the inhibitory effects of hyperpolarization. This mechanism is likely to contribute to the inhibitory effects of I_h on dendritic excitability seen in a wide variety of neurons. Moreover, regulation of HCN channel function by modulatory transmitters may provide an important physiological mechanism to dynamically control Ca²⁺-dependent processes at distal dendrites.

RESULTS

Whole-cell recordings were obtained from CA1 pyramidal neurons in acute hippocampal slices from wild-type (WT)

and HCN1 KO ($-/-$) mice (Nolan et al., 2003). Neurons were loaded with a low-affinity Ca²⁺-indicator dye (Oregon Green BAPTA-5N) and a Ca²⁺-independent dye (Alexa Fluor 594) to monitor dendritic structure (Figure 1A; Experimental Procedures). Local PP inputs were activated by a glass bipolar stimulating patch electrode placed within 50–100 μ m of the targeted branch under visual guidance (Figure 1A). The somatic voltage response was recorded under current-clamp conditions, with inhibitory synaptic transmission blocked using both GABA_A and GABA_B receptor antagonists. At the same time we used two-photon microscopy to measure the Ca²⁺ signals in the distal CA1 dendrites in stratum lacunosum-moleculare (SLM), at least 50 μ m past the main branching point of the distal dendritic tuft (>400 μ m from the soma).

Burst Stimulation of PP Inputs Elicit Nonlinear Dendritic Calcium Events in SLM Dendrites

We first characterized the Ca²⁺ events induced in distal dendrites in response to a brief burst of PP synaptic stimulation (ten stimuli at 100 Hz) similar to that used during induction of PP LTP (Nolan et al., 2004). The burst stimulus elicited a large transient increase in the Ca²⁺ fluorescence signal in a continuous segment of SLM dendrite during 2D scanning (~ 8 Hz) (Figure 1B). Ca²⁺ increases were observed in both spines and dendrite shafts. However, segments proximal to the active portion of a dendrite or on adjacent branches showed little or no Ca²⁺ increase, indicating that the Ca²⁺ event was localized to the distal dendritic branch.

Previous studies in rat hippocampal slices found that local glutamate application to distal CA1 neuron dendrites (Cai et al., 2004; Wei et al., 2001) or burst stimulation of distal synapses (Golding et al., 2002) can elicit local dendritic Ca²⁺ action potentials. To determine whether the signals we observed in mouse hippocampal slices also represent dendritic Ca²⁺ spikes, we asked whether the responses displayed properties consistent with regenerative activity. The peak Ca²⁺ signal in the distal dendritic shaft (measured by the change in Oregon Green/Alexa 594 fluorescence ratio, normalized to baseline, $\Delta S/S_0$; see Experimental Procedures) was quantified on a fast timescale using linescan mode (500 Hz sampling). There was a steep sigmoidal relationship between current stimulus intensity and peak fluorescence change (Figures 1C and 1D), indicative of a nonlinear regenerative response. At low stimulus intensities (typically <40 μ A) there was little dendritic fluorescence change despite a measurable somatic depolarization (Figure 1E), consistent with the need for recruitment of a threshold number of distal inputs. The peak Ca²⁺ change reached a maximum value of $100.4\% \pm 8.9\%$ at high stimulus intensities (Figure 1D; $n = 22$). In contrast, the peak somatic voltage response continued to increase with increasing stimulus strength (Figure 1F), perhaps reflecting the further recruitment of synapses and/or Ca²⁺ spikes at different dendritic branches.

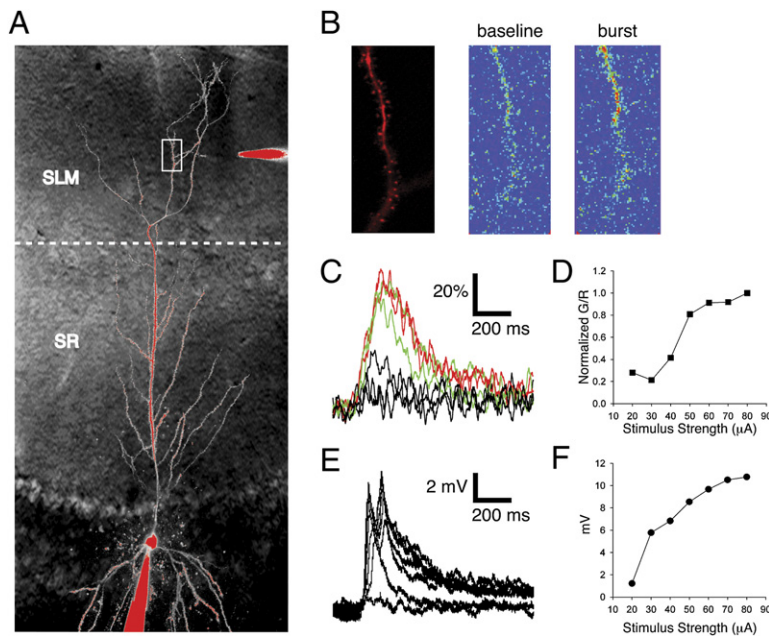


Figure 1. Burst Stimulation of PP Inputs Elicits Nonlinear Distal Ca²⁺ Events

(A) Schematic of experiment. Whole-cell recordings of CA1 pyramidal neurons were obtained using a patch pipette (bottom of image) filled with a Ca²⁺-independent red fluorescent dye (25 μM Alexa 594; signal R) and a Ca²⁺-indicator green fluorescent dye (500 μM OGB-5N; signal G). An extracellular stimulating electrode (top of image) filled with Alexa 594 was placed ~50 μm from a dendrite of interest (white box) in stratum lacunosum-moleculare (SLM) under two-photon visual guidance. (B) Visualization of SLM dendrite segment using a 2D scan. (Left) Image of dendrite morphology. (Right) Ca²⁺-sensitive fluorescence before (left) and during (right) a Ca²⁺ spike induced by synaptic stimulation (ten stimuli at 100 Hz). Pseudocolor image in which warmer colors indicate brighter Ca²⁺ dye fluorescence. Differences in resting fluorescence reflect degree to which dendrite region is in focal plane. (C) Ca²⁺ signal transients with burst stimulation using 40, 50, and 60 μA currents measured in linescan mode through dendritic shaft, expressed as percent change in G/R (defined as $\Delta S/S_0 \times 100\%$, where $S = G/R$; see [Experimental Procedures](#)).

(D) Plot of normalized peak Ca²⁺ signal versus stimulus current. Distal Ca²⁺ signals show a nonlinear sigmoidal dependence on stimulus current.

(E) Voltage responses to PP burst stimulation corresponding to Ca²⁺ signals in panel (D).

(F) Plot of peak depolarization (from panel [E]) versus stimulus current.

The Ca²⁺ events had a remarkably long duration, with a mean half-width of 315.5 ± 23.6 ms. Often a plateau phase was observed that was followed by a faster decay to baseline, with an 80%–20% decay time of 258.8 ± 31.7 ms (Figure 2A, black). In contrast, the Ca²⁺ signals rose more rapidly (77.8 ± 4.84 ms; 20%–80% rise time), comparable to the duration of the stimulus burst. The time course of these Ca²⁺ signals is similar to that of the distal Ca²⁺ spikes observed in rat slice cultures (Cai et al., 2004; Wei et al., 2001) but is much longer than the dendritic Ca²⁺ spikes observed in the distal apical trunk of CA1 neurons in stratum radiatum (Golding et al., 2002; Schiller et al., 1997). Such long events may reflect unique properties of voltage-gated channels at more terminal apical dendrites (Cai et al., 2004) and/or the large NMDA/AMPA receptor ratio found at perforant path synapses (Nicholson et al., 2006; Otmakhova et al., 2002).

Given the long duration and large amplitude of these Ca²⁺ signals, it was important to verify that the dye was not saturated. We therefore measured the maximal Ca²⁺ signal under saturating conditions in response to steady-state bath application of the Ca²⁺ ionophore ionomycin in the presence of 2 mM external Ca²⁺ (Figure S1 available online). The peak Ca²⁺ signal elicited by a synaptic burst was equal to $44.9\% \pm 7.9\%$ of the maximum signal with ionomycin, indicating that slightly less than half of the dye molecules were complexed with Ca²⁺. Based on our measured value for the K_d of the dye of 13.4 μM (Figure S1), we calculate that the fluorescence change elicited

by a synaptic burst corresponded to a peak free [Ca²⁺] value of ~11 μM, a postsynaptic level sufficient for induction of LTP (Yang et al., 1999).

Despite the relatively strong synaptic stimulation, the somatic voltage responses were usually subthreshold (Figure 1E, F), with axonal spiking observed in only 8 out of 22 cells. On average, the absolute somatic depolarization reached 12.0 ± 0.8 mV, with a fast rise (60.14 ± 7.3 ms) and slower decay (80%–20%) time (490 ± 40.7 ms). These results are consistent with previous findings that SLM inputs are typically weak and inefficient at driving somatic spikes (Golding and Spruston, 1998; Jarsky et al., 2005) but can elicit long-lasting distal Ca²⁺ spikes (Cai et al., 2004; Wei et al., 2001). It is likely that the local depolarization in the distal dendrite is several-fold greater than that observed in the soma and sufficient for triggering regenerative activity, given the attenuation of voltage signals along apical CA1 dendrites (Golding et al., 2005).

Deletion of HCN1 Enhances Both Peak Amplitude and Duration of Distal Dendritic Ca²⁺ Events

To examine the influence of HCN1 on distal dendritic excitability, we compared the dendritic Ca²⁺ events in HCN1 knockout (KO) mice to those in wild-type (WT) littermates. Similar to previous results (Nolan et al., 2004), we found that the somatic resting potential of the KO mice (-74.9 ± 2.4 mV, $n = 6$) was significantly more negative than that of wild-type mice (-68.1 ± 1.3 mV, $n = 6$). Despite this hyperpolarization, PP stimulation elicited a Ca²⁺

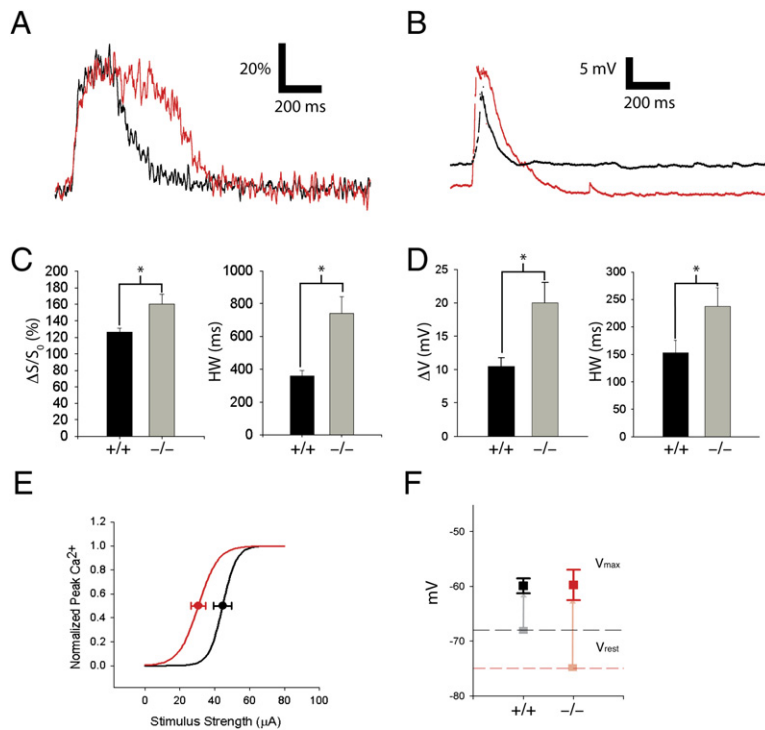


Figure 2. HCN1 Deletion Increases Magnitude and Prolongs Duration of Distal Ca²⁺ Events

(A) Distal Ca²⁺ transient in SLM dendrites in HCN1 knockout mouse (KO; red trace) and wild-type littermate (WT; black). Vertical scale bar represents fluorescence signal ($\Delta S/S_0 \times 100\%$).

(B) Somatic voltage in response to PP burst stimulation in KO and WT mice. Note that resting potential in KO mice was hyperpolarized relative to WT mice by 7 mV.

(C) Mean peak Ca²⁺ signal and duration in KO mice (–/–) versus WT littermates (+/+). ($\Delta S/S_0$: WT = $131.8 \pm 8.5\%$, $n = 7$; KO = 174.8 ± 15.0 , $n = 7$; $p < 0.03$; unpaired t test; Half-width: WT = 340 ± 33.7 ms; KO: HW = 768 ± 93.3 ms; $p < 0.01$). Error bars represent standard error. Asterisks denote statistical significance.

(D) Mean somatic voltage responses in KO versus WT mice. Peak depolarization (ΔV): WT = 8.6 ± 0.7 mV; KO = 16.3 ± 1.9 mV. Half-width: WT = 224.8 ± 21.9 ms; KO = 367.9 ± 52.3 ms. Error bars represent standard error. Asterisks denote statistical significance.

(E) Effect of HCN1 deletion on peak Ca²⁺ response versus stimulus current relation. Average sigmoid relationship between peak Ca²⁺ and stimulus strength in KO (red) and WT (black) littermates from fits of Boltzmann

relation to individual curves. The KO mice exhibit a slight left-shifted half-maximal stimulus value ($I_{1/2}$: WT = 45.2 ± 3.0 μA [$n = 5$]; KO = 35.2 ± 3.8 μA [$n = 5$]; $p = 0.075$). The slopes (k) of the relationships were not significantly different (k : WT = 3.9 ± 1.2 ; KO = 5.6 ± 1.9 ; $p = 0.45$).

(F) Effect of HCN1 deletion on resting potential (light squares, dashed lines) and peak EPSP voltage (solid squares). Resting potentials (V_{rest}) were more negative in KO mice relative to WT mice (WT: $V_{rest} = -68.1 \pm 1.3$ mV, $n = 6$; KO: $V_{rest} = -74.9 \pm 2.4$ mV, $n = 6$; $p < 0.05$). The peak potential during EPSP elicited by PP burst stimulation (V_{peak}) was similar in WT and KO neurons (WT: $V_{peak} = -59.9 \pm 1.4$ mV [$n = 6$]; KO: $V_{peak} = -59.7 \pm 2.8$ mV [$n = 6$]; $p = 0.96$). Vertical lines indicate the magnitude of depolarization due to the burst stimulus. Error bars represent standard error.

transient in the distal dendrites of the KO mice that was both larger in peak amplitude and strikingly longer in duration than the corresponding signals from WT littermates (Figures 2A and 2C).

Deletion of HCN1 increased the peak Ca²⁺ signal ($\Delta S/S_0$) by ~30%, from $131.8 \pm 8.5\%$ ($n = 7$) in WT mice to $174.8 \pm 15.0\%$ ($n = 7$) in KO mice ($p < 0.03$, Student's t test). The effect on duration was even more dramatic, with half-width increasing over 2-fold, from 340 ± 33.7 ms in the WT mice to 768 ± 93.3 ms in the mutants ($p < 0.01$). The somatic voltage responses to PP burst stimulation displayed a similar trend (Figures 2B and 2D), with the KO mice exhibiting a larger peak depolarization (16.3 ± 1.9 mV) and longer half-width (367.9 ± 52.3 ms) compared to the values in WT mice (8.6 ± 0.7 mV and 224.8 ± 21.9 ms). There was no significant difference in either Ca²⁺ rise times (WT: 51 ± 4.7 ms versus KO: 68 ± 8 ms; $p > 0.05$) or 80%–20% decay times (WT: 300 ± 38.7 ms, KO: 442.3 ± 82.8 ms; $p > 0.05$) between genotypes, suggesting that the prolonged time course of the distal events was not due to altered Ca²⁺ buffering and/or extrusion.

The similarity of decay times of the Ca²⁺ transients indicates that the major effect of the KO was to prolong the

duration of the plateau phase and increase its amplitude. Based on the dye K_d , the 30% increase in peak fluorescence change upon HCN1 deletion represents a 70% increase in peak $[Ca^{2+}]_i$, to a value of 18.9 μM , consistent with the increase in PP LTP in the HCN1 KO mice (Nolan et al., 2004).

To determine whether deletion of HCN1 lowers the threshold current for generating Ca²⁺ spikes, we compared the relationship between peak Ca²⁺ and stimulus intensity in WT versus KO mice (Figure 2E). HCN1 deletion showed a trend to produce a small decrease in the stimulus current needed to elicit distal Ca²⁺ events, with KO mice exhibiting a half-maximum stimulus current ($I_{1/2} = 35.2 \pm 3.8$ μA , $n = 5$) that was ~22% lower than the value in WT mice ($I_{1/2} = 45.2 \pm 3.0$ μA , $n = 5$), although the difference did not attain statistical significance ($p = 0.075$). The peak somatic voltage during the burst EPSP was also relatively unchanged by HCN1 deletion (Figure 2F; peak voltage = -59.9 ± 1.4 mV in WT versus -59.7 ± 2.8 mV in KO mice; $p = 0.96$), consistent with a relatively unchanged threshold. The lack of change in absolute peak EPSP voltage is likely due to the offsetting effects of enhanced integration (due to the increase in input resistance) versus membrane hyperpolarization upon HCN1 deletion.

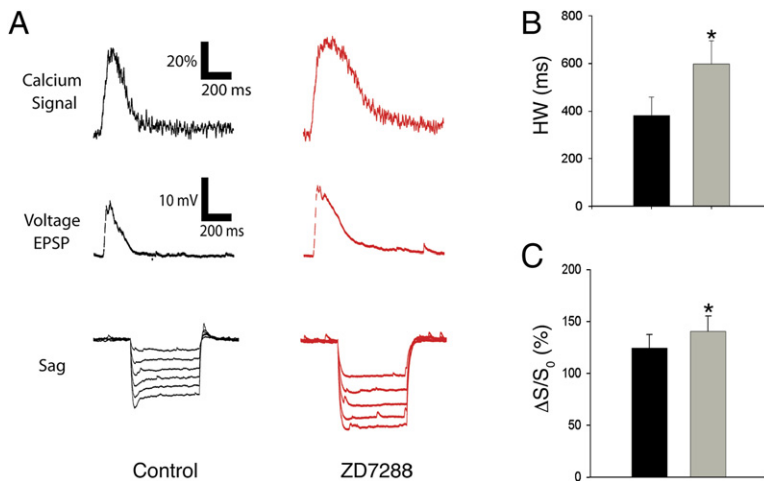


Figure 3. Pharmacological Blockade of I_h with ZD7288 Increases Amplitude and Duration of Distal Ca²⁺ Events

(A) Example Ca²⁺ (top) and somatic voltage (middle) responses from a WT mouse to PP burst stimulation in the absence (black) and presence (red) of ZD7288 (10 μM). (Bottom) Hyperpolarization-induced voltage sag due to activation of I_h in response to current steps from -20 to -120 pA was blocked with ZD7288.

(B) Average half-width of distal Ca²⁺ events before and after application of ZD7288. Duration of Ca²⁺ transients was significantly prolonged (+57%) by ZD7288 (Control: HW = 345.1 ± 74.6 ms; ZD7288: HW = 541.7 ± 99.2 ms; p < 0.01). Error bars represent standard error. Asterisks denote statistical significance compared to control.

(C) Average peak Ca²⁺ before and after application of ZD7288. Peak Ca²⁺ levels were increased by ~17% in drug (Control: ΔS/S₀ = 109.4% ± 18.6%; ZD7288: ΔS/S₀ = 127.9% ± 17.8%; n = 7; paired t test, p < 0.01). Error bars represent standard error. Asterisks denote statistical significance compared to control.

Pharmacological Blockade of I_h Enhances Distal Dendritic Calcium Events Specifically in the Perforant Path

The dramatic prolongation and enhancement of the distal Ca²⁺ transients in the HCN1 KO mice is surprising given that the HCN1 channels generate a depolarizing current and, moreover, should rapidly shut off within ~20–50 ms during depolarizing events (Magee, 1998). Since gene deletions can result in reactive changes in expression of other gene products, we tested the effects of acute pharmacological blockade of I_h in WT mice with the organic antagonist ZD7288. To minimize nonspecific actions of this compound on synaptic transmission (Chen, 2004; Chevaleyre and Castillo, 2002) and other channels (Felix et al., 2003), we used relatively low concentrations of drug (10 μM) and short times of exposure (10–15 min) that were just sufficient to eliminate the characteristic I_h-dependent depolarizing sag in voltage in response to a somatic hyperpolarizing current step (Figure 3A).

Acute application of ZD7288 under these conditions produced similar changes in the distal dendritic Ca²⁺ transient to those seen upon deletion of HCN1 (Figure 3). Thus we observed an ~17% increase in peak Ca²⁺ signal, from 109.4% ± 18.6% in the absence of drug to 127.9% ± 17.8% in the presence of ZD7288 (n = 7; p < 0.01). We also found an ~57% prolongation in the Ca²⁺ signal duration, from 345.3 ± 74.6 ms in the absence of drug to 541.7 ± 99.2 ms in the presence of blocker (p < 0.01). Ca²⁺ rise and decay times in control conditions (τ_r = 72.33 ± 9.07 ms, τ_d = 275 ± 97.01) and in the presence of ZD7288 (τ_r = 109.75 ± 6.38 ms, τ_d = 464.33 ± 103.12 ms) showed no statistically significant differences, similar to results with HCN1 deletion. The similarity in effects of reducing I_h either by phar-

macological or genetic means suggests that the enhancement in dendritic Ca²⁺ events reflects a specific effect due to the loss of I_h, rather than a nonspecific effect or compensatory change in other channels.

If the enhancement in distal dendritic Ca²⁺ signals is indeed causally related to the loss of local I_h, then ZD7288 should produce much less of a change in Ca²⁺ signals observed in stratum radiatum (SR) in response to SC stimulation, as the levels of HCN1 and I_h are much lower in proximal dendrites than in distal dendrites. Indeed, burst stimulation of SC inputs identical to that used in the PP experiments elicited a proximal Ca²⁺ response in SR that showed little change following blockade of I_h with ZD7288 (Figure 4A1 traces). There was, if anything, a small, statistically insignificant, decrease in Ca²⁺ signal duration (Figure 4B; Control HW = 150.67 ms ± 4.64 ms; ZD7288 HW = 144 ± 2.26 ms, n = 6, p = 0.14) and peak amplitude (Figure 4C; Control ΔS/S₀ = 292.59% ± 29.8%, ZD7288 ΔS/S₀ = 226.36% ± 35.1%, p = 0.08). The lack of augmentation of the Ca²⁺ signal elicited by SC stimulation was not due to use of the higher-affinity Ca²⁺ dye, Fluo-4, in these experiments (needed to measure the lower-amplitude proximal Ca²⁺ signals), as Fluo-4 detected a large prolongation in Ca²⁺ event duration at the distal dendrites in response to PP stimulation (Figures 4A2 and 4B; Control HW = 558.6 ms ± 118.11, ZD7288 HW = 995 ± 245.53 ms, p < 0.01). However, the peak of the Fluo-4 Ca²⁺ signal in the distal dendrites did not show an augmentation following I_h blockade (Control 146.33% ± 17.7%, ZD7288 145.27% ± 14.1%; p = 0.92), most likely due to saturation of the higher-affinity dye by the very large distal Ca²⁺ transient. The selective ability of ZD7288 to enhance the distal but not proximal

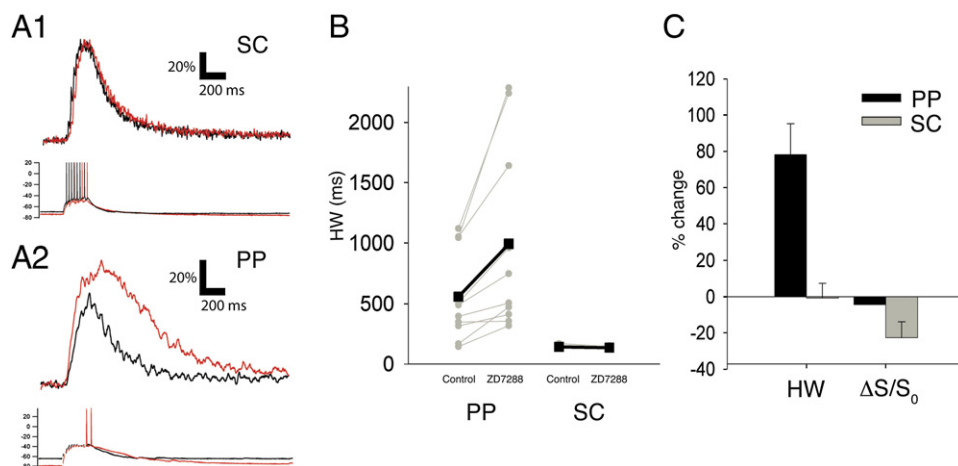


Figure 4. Blockade of I_h Prolongs Ca²⁺ Signals Elicited by Perforant Path but Not Schaffer Collateral Stimulation

Dendritic Ca²⁺ signals in proximal or distal CA1 dendrites in response to 100 Hz burst stimulation (10 stimuli) of SC or PP inputs, respectively, under control conditions (black) or in the presence of 10 μ M ZD7288 (red). Ca²⁺ signals were measured with higher affinity Ca²⁺ dye, Fluo-4 (400 μ M).

(A1) Effects of ZD7288 on proximal dendritic Ca²⁺ signals (top) and somatic voltage response (bottom) elicited by stimulation of SC synapses. (A2) Effects of ZD7288 on distal dendritic Ca²⁺ signals and somatic voltage response induced by burst stimulation of PP inputs. Distal but not proximal Fluo-4 Ca²⁺ signals are prolonged by ZD7288.

(B) Effects of ZD7288 on Fluo-4 Ca²⁺ signal half-width duration in distal dendrites in response to PP stimulation or in proximal dendrites in response to SC stimulation. Grey symbols and lines show half-width durations for each individual experiment. Black symbols and lines show mean values. Values for distal dendrites in response to PP stimulation: Control: HW = 558.6 \pm 118.11 ms; ZD7288: HW = 995 \pm 245.53 ms; n = 10; p < 0.01, paired t test. Values for SR dendrites with SC stimulation: Control: HW = 150.67 \pm 4.64 ms; ZD7288: HW = 144 \pm 2.26 ms; n = 6, p = 0.14.

(C) Summary of effects of ZD7288 on HW and peak Ca²⁺ signals ($\Delta S/S_0$) elicited by PP (Control: $\Delta S/S_0$ = 146.3% \pm 17.7%, ZD7288: $\Delta S/S_0$ = 145.3% \pm 14.1%; p = 0.92) and SC stimulation (Control $\Delta S/S_0$ = 292.59% \pm 29.8%, ZD7288 $\Delta S/S_0$ = 226.36% \pm 35.1%, p = 0.08). Error bars represent standard error.

Ca²⁺ signal supports the view that the calcium enhancement induced by HCN channel blockade is due to the local reduction of I_h .

Does the prolongation of the distal Ca²⁺ signal reflect a prolongation of the distal voltage response to synaptic stimulation? We examined this question by obtaining whole-cell dendritic voltage recordings in mid to distal SR (85 and 200 μ m from the soma) (Figure 5A). Consistent with our imaging data, PP burst stimulation elicited large, long-lasting depolarizing responses in the dendrites, and these responses were significantly prolonged by ZD7288 (10 μ M) (Figures 5B1-2 and C1-2). This prolongation was primarily due to an increase in the afterdepolarization following the end of stimulation, indicating an increase in local excitatory dendritic current. In contrast, ZD7288 produced little prolongation of the dendritic voltage response to SC stimulation, consistent with a specific effect due to I_h blockade (Figures 5D1 and 5D2).

Pharmacological Analysis of Distal Ca²⁺ Events in SLM

Which ion channels and receptors mediate the distal Ca²⁺ events and regulate their properties by interacting with I_h ? We first examined the importance of ionotropic glutamate receptors, which have been previously shown to trigger distal Ca²⁺ spikes (Golding et al., 2002; Wei et al., 2001). Bath application of APV (50 μ M) or CNQX (10 μ M) to block NMDA receptors or AMPA receptors, respectively, caused a substantial reduction in both the peak somatic

voltage response and amplitude of the distal Ca²⁺ signal in response to a burst of PP stimulation (Figures 6A, 6B, and 6G). Thus, application of APV reduced the Ca²⁺ signal ($\Delta S/S_0$) to 11.9% \pm 2.3% of its control value (p < 0.01, n = 5) and decreased peak somatic voltage amplitude to 62.5% \pm 5.0% of control (p < 0.05, n = 5). Similarly, CNQX reduced the Ca²⁺ signal to 24.5% \pm 8.8% (n = 4, p < 0.05) and voltage amplitude to 26.5% \pm 10.0% (n = 4, p < 0.05) of their initial levels, indicating the importance of both AMPA and NMDA receptors.

Are NMDA receptors sufficient for generating the local nonlinear Ca²⁺ signals, as found for Ca²⁺ spikes in basal dendrites of neocortical pyramidal neurons (Schiller et al., 2000), or are other sources of Ca²⁺ also required? We first examined the involvement of Ni²⁺-sensitive and L-type voltage-gated Ca²⁺ channels, which have been implicated in distal LTP (Golding et al., 2002; Remondes and Schuman, 2003). However, combined application of 50 μ M Ni²⁺ (an inhibitor of R- and T-type VGCCs) and 20 μ M nimodipine (a dihydropyridine L-type VGCC blocker) had little effect on either the dendritic Ca²⁺ signal ($\Delta S/S_0$ = 99.3% \pm 3.6% of control) or on the somatic EPSP (ΔV = 86.1% \pm 4.6% of control, n = 4, p = 0.89) in response to a burst of PP stimuli (Figures 6C and 6G). This finding is in contrast to the sensitivity of Ca²⁺ transients in SR to these antagonists, as previously reported (Christie et al., 1995) and confirmed by our own experiments (Figure S4).

We next focused on the Ca_v3.3 T-type channels and N-type channels, two types of Ni²⁺- and

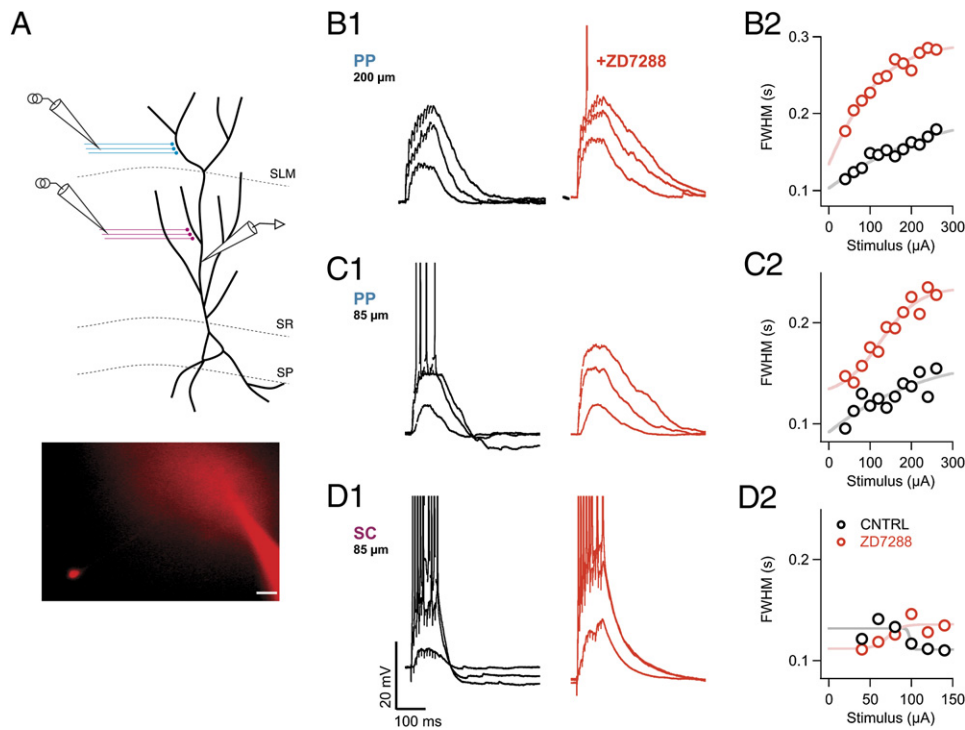


Figure 5. Acute Blockade of I_h Prolongs Duration of the Long-Lasting Dendritic Depolarization in Response to PP but Not SC Stimulation

(A) Schematic of the recording configuration. Whole-cell current-clamp voltage recordings were obtained from the apical trunk of a CA1 pyramidal neuron dendrite. Extracellular electrodes were positioned to stimulate either PP inputs in SLM or SC inputs in SR. (Inset) Brightfield Alexa 594 fluorescent image of a representative recording. Soma of patch-clamped dendrite is visible in the CA1 pyramidal cell layer. Scale bar, 20 μ m.

(B1) Voltage responses to low, intermediate, or strong PP stimulation from a whole-cell dendritic recording obtained \sim 200 μ m from the center of the soma, in the absence (black traces) or presence (red traces) of ZD7288 (10 μ M).

(C1) Voltage responses in absence or presence of ZD7288 to low, intermediate, or strong PP stimulation from a second dendritic recording \sim 85 μ m from soma.

(D1) Dendritic voltage responses to SC stimulation from same recording shown in (C) in the absence and presence of ZD7288.

(B2–D2) Plots of full-width half-maximum (FWHM) duration of voltage responses as function of stimulus intensity in the absence (black circles) or presence (red circles) of ZD7288 for experiments shown in (B1)–(D1).

nimodipine-insensitive VGCCs that are expressed in distal CA1 dendrites (McKay et al., 2006; Mills et al., 1994; Westebroek et al., 1992). Indeed, the peak Ca²⁺ transients were substantially reduced by application of either the general T-type channel antagonist mibefradil (Figures 6E and 6G; $\Delta S/S_0 = 53\% \pm 11.4\%$ of control, $p < 0.05$; $n = 5$) or by the N-type channel antagonist ω -conotoxin GVIA (Figures 6D and 6G; $\Delta S/S_0 = 57.3\% \pm 9.6\%$ of control, $p < 0.05$; $n = 5$). However, the peak EPSP at the soma was only slightly reduced by either mibefradil (EPSP = $80\% \pm 9.9\%$ of control, $n = 5$) or ω -conotoxin GVIA (EPSP = $90.8\% \pm 14.5\%$ of control, $n = 4$) (Figures 6D, 6E, and 6G). Importantly, neither agent caused a significant change in the PP field EPSP (Figure S2), indicating that they did not alter transmitter release from the PP terminals (or cause significant block of AMPA or NMDA receptors). Thus, the distal Ca²⁺ spikes appear to recruit both Ca_v3.3 T-type and Ca_v2.2 N-type voltage-gated Ca²⁺ channels. Although mibefradil can also block L-type and R-type VGCCs (Randall and Tsien, 1997), our

finding that the distal Ca²⁺ events are insensitive to Ni²⁺ and high concentrations of nimodipine indicates that the effects of mibefradil do indeed reflect T-type channel blockade. We also think it unlikely that the effects of mibefradil are due to block of voltage-gated Na⁺ channels (Eller et al., 2000), since we find that low concentrations of TTX (30 nM) that preferentially block dendritic Na⁺ spikes (Gasparini et al., 2004) do not reduce the amplitude of the local distal Ca²⁺ signal (Figure S5). Finally, we found that Ca²⁺ release from intracellular stores does not contribute to the distal Ca²⁺ signals, because blockade of the smooth endoplasmic reticulum Ca²⁺ (SERCA) pump with 30 μ M cyclopiazonic acid (CPA) had no effect on the distal Ca²⁺ transient (Figures 6F and 6G; $\Delta S/S_0 = 110.7\% \pm 14.4\%$ of control, $n = 6$, $p = 0.42$).

A Computational Model for the Enhancement in the Distal Ca²⁺ Transient upon I_h Blockade

To gain further insight into the mechanism by which I_h blockade alters the distal Ca²⁺ transients, we developed

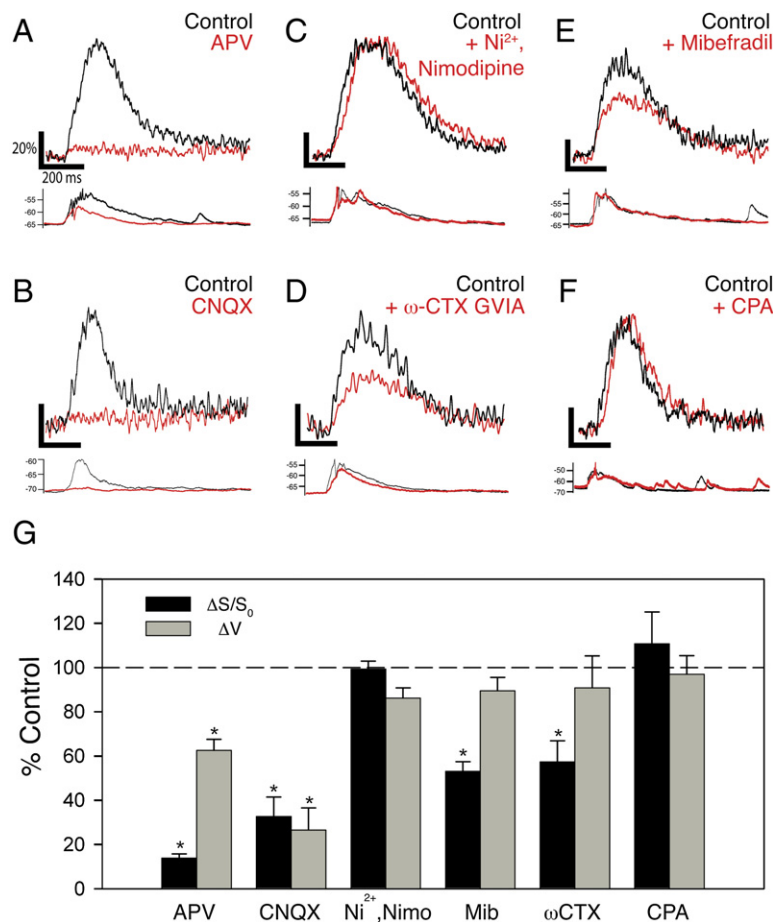


Figure 6. Ca²⁺ Signals in Distal Dendrites Are Initiated by Activation of NMDA and AMPA Receptors, and Mediated by Ni²⁺-Insensitive T-Type and N-Type Voltage-Gated Ca²⁺ Channels

(A–F) Examples of effects of pharmacological agents on distal Ca²⁺ signals (top) and somatic voltage responses (bottom) elicited by burst stimulation of PP inputs. Black, control traces. Red, traces obtained in the presence of the following blockers: (A) 50 μ M D-APV, an NMDAR antagonist; (B) 20 μ M CNQX, an AMPAR antagonist; (C) combination of 50 μ M Ni²⁺ (Ca_v3.2 T-type and R-type VGCC antagonist) and 20 μ M nimodipine (L-type VGCC antagonist); (D) 1 μ M ω -conotoxin GVIA, N-type VGCC antagonist; (E) 20 μ M mibefradil, general T-type channel antagonist; and (F) 30 μ M cyclopiazonic acid, a blocker of the SERCA pump.

(G) Summary of effects of pharmacological inhibitors on distal Ca²⁺ signal (black) and somatic voltage response (gray). Asterisks denote statistical significance comparing drug versus control ($p < 0.05$). D-APV: Ca²⁺ signal ($\Delta S/S_0$) reduced to 11.9% \pm 2.3% of control ($p < 0.01$, $n = 5$); $\Delta V = 62.5\% \pm 5.0\%$ of control ($p < 0.05$, $n = 5$). CNQX: $\Delta S/S_0 = 32.7\% \pm 8.7\%$ of control ($p < 0.01$, $n = 4$); $\Delta V = 26.5\% \pm 10.0\%$ of control ($p < 0.05$, $n = 4$). Ni²⁺ + nimodipine: $\Delta S/S_0 = 99.3\% \pm 3.6\%$ of control; $\Delta V = 86.1\% \pm 4.6\%$ of control ($p > 0.1$ for both; $n = 4$). Mibefradil: $\Delta S/S_0 = 53\% \pm 11.4\%$ of control, $p < 0.05$; $\Delta V = 80\% \pm 9.9\%$ of control ($p > 0.1$; $n = 4$). ω -CTX GVIA: $\Delta S/S_0 = 57.3\% \pm 9.6\%$ of control, $p < 0.05$; $\Delta V = 90.8\% \pm 14.5\%$ of control, $p > 0.1$ ($n = 4$). CPA: $\Delta S/S_0 = 110.7\% \pm 14.4\%$ of control ($p = 0.42$; $n = 6$). Error bars represent standard error.

a computational model representing an active distal dendritic branch with voltage-gated conductances, including T-type and N-type VGCCs (see Supplemental Section 2). In the presence of I_h , a simulated burst of synaptic activation of NMDA and AMPA receptors on the dendritic branch evoked a strong depolarization that triggered a nonlinear long-lasting spike (Figure 7A1). Removal of I_h hyperpolarized the resting membrane by ~ 6 mV, similar to the hyperpolarization observed in HCN1 KO mice (Nolan et al., 2004). Strikingly, the same synaptic stimulation elicited a local Ca²⁺ spike whose duration was enhanced nearly 2-fold, with a smaller increase in peak amplitude. In agreement with our somatic voltage recordings, blockade of I_h did not affect the peak absolute voltage reached during the burst of EPSPs prior to the spike, indicating that the hyperpolarization upon loss of I_h is offset by an increase in EPSP amplitude and temporal summation due to the increase in input resistance. Interestingly, when we examined a morphologically realistic model of a CA1 neuron, I_h blockade produced changes in somatic voltage responses similar to our experimental data (Figure S3).

Next we focused on the single-compartment model to gain insight into how removal of I_h altered the local Ca²⁺

transient in the distal dendrites. Blockade of I_h nearly doubled the peak Ca²⁺ current carried by the N- and T-type VGCCs during a dendritic spike (95% increase) and markedly prolonged the duration of Ca²⁺ influx (Figure 7A2). Furthermore, when we included a Ca²⁺ dye and endogenous Ca²⁺ buffering and transport in the model to calculate the Ca²⁺ fluorescence signal (Figure 7A3; see Supplemental Material Section 2), removing I_h produced a large (90%) increase in the peak Ca²⁺ signal and a 2-fold prolongation of its duration (116% increase in HW) (Figure 7A3), similar to our experimental findings (Figures 2 and 3). Importantly, these modeling results were robust, as they were observed over a wide range of parameter space for the voltage-gated Ca²⁺ channel kinetics (data not shown).

What is responsible for the pronounced increase in Ca²⁺ influx during the dendritic spikes in response to removal of I_h ? Analysis of the T-type and N-type VGCCs gating parameters revealed that the voltage-dependent activation of both channels was similar during the Ca²⁺ spikes in the presence and absence of I_h . However, the fraction of inactivated channels both before and during the spikes was significantly less when I_h was removed (Figure 7A4), due to the hyperpolarization of the resting membrane.

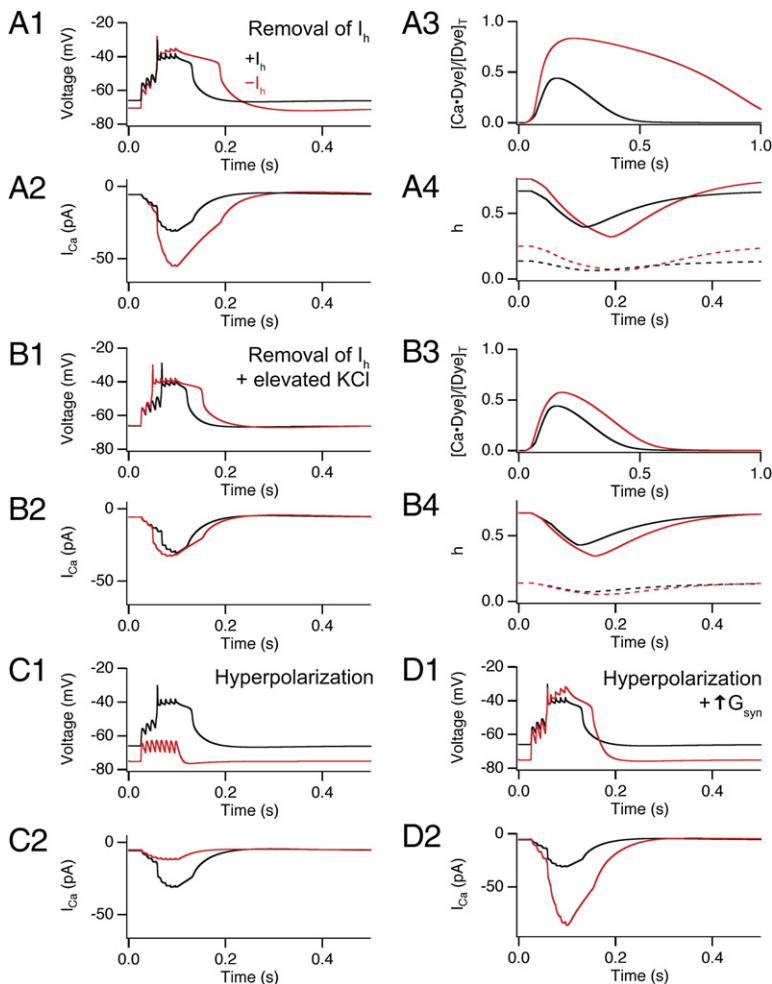


Figure 7. Computational Model of Distal Ca²⁺ Events and Effects of I_h Blockade

(A and B) Results from a single-compartment model for Ca²⁺ spike elicited by PP burst stimulation showing distal dendritic membrane voltage (panels labeled 1), total VGCC current (panels labeled 2), Ca²⁺-bound fraction of dye (panels labeled 3), and T-type and N-type VGCC inactivation gating variable (*h*, panels labeled 4). Simulations shown in the presence (black traces) or absence (red traces) of I_h. (A) Effects of I_h removal. (A1) Burst of 100 Hz synaptic stimulation evoked a nonlinear voltage response (Ca²⁺ spike). Removal of I_h hyperpolarized the resting membrane and enhanced the duration of Ca²⁺ spike. (A2) The sum of T-type and N-type Ca²⁺ current during Ca²⁺ spike shows enhanced Ca²⁺ influx upon removal of I_h. (A3) The fraction of Ca²⁺-bound indicator dye is enhanced and prolonged upon removal of I_h, similar to our experimental results. (A4) Plot of inactivation gating variable *h* for T-type and N-type VGCCs before (starting values) and during Ca²⁺ spike (solid lines, N-type; dashed lines, T-type), showing decreased inactivation upon removal of I_h. Note: *h* = 1 when all inactivation gates are open. (B) Effects of I_h removal when membrane hyperpolarization is prevented by shifting the reversal potential of the leak conductance from -80.0 to -72.9 mV. Parameters defined as in (A). Error bars represent standard error. (C) Effects of membrane hyperpolarization alone in maintained presence of I_h. Black traces, control. Red traces, during injection of a -0.011 nA hyperpolarizing current. (D) Effect of membrane hyperpolarization in maintained presence of I_h but with a 60% increase in excitatory synaptic conductance to trigger a dendritic Ca²⁺ spike. Black and red traces in the absence and presence of -0.011 nA current. Error bars represent standard error.

This effect produced an 84% increase in availability of T-type channels and a 14% increase in availability of N-type channels prior to the spike.

Since loss of I_h both hyperpolarizes the resting membrane and increases the input resistance, we used the model to dissect the relative importance of these two effects. We first asked whether hyperpolarization is necessary for the enhancement in the Ca²⁺ signal. Following removal of I_h, the membrane was depolarized back to its original potential by adjusting the K⁺ reversal potential (E_K) to a more positive value (E_K = -72.9 mV). Under these conditions where I_h was absent but resting potential was unchanged, the model generated a nearly normal-sized Ca²⁺ influx and Ca²⁺ signal even though there was still a significant increase in input resistance due to the lack of I_h (Figure 7B). Thus, membrane hyperpolarization is necessary for the enhancement.

We then tested whether hyperpolarization alone is sufficient to enhance the distal Ca²⁺ spike. A normal-sized I_h was maintained in the simulation while the membrane

was hyperpolarized to a negative potential equal to that normally reached upon I_h removal. Although steady-state availability of T- and N-type channels was increased to a similar extent as seen upon removal of I_h, the burst of EPSPs failed to trigger a Ca²⁺ spike because the peak EPSP voltage was now subthreshold (Figure 7C). This is in contrast to our experimental results where loss of I_h had little effect on the threshold for eliciting a dendritic spike (Figure 2). To counteract the inhibitory effect of the hyperpolarization, we increased the size of the synaptic conductance to reach a peak voltage similar to that seen when EPSPs are elicited from the normal resting potential. Under these conditions, the model dendrite generated a Ca²⁺ signal with a significantly enhanced amplitude and duration, similar to that observed in the absence of I_h (Figure 7D). Thus, spike prolongation does not require the increase in input resistance associated with the removal of I_h, as long as the EPSP is large enough to reach threshold.

These simulation results indicate that the effect of I_h removal to enhance the Ca²⁺ spikes depends on two

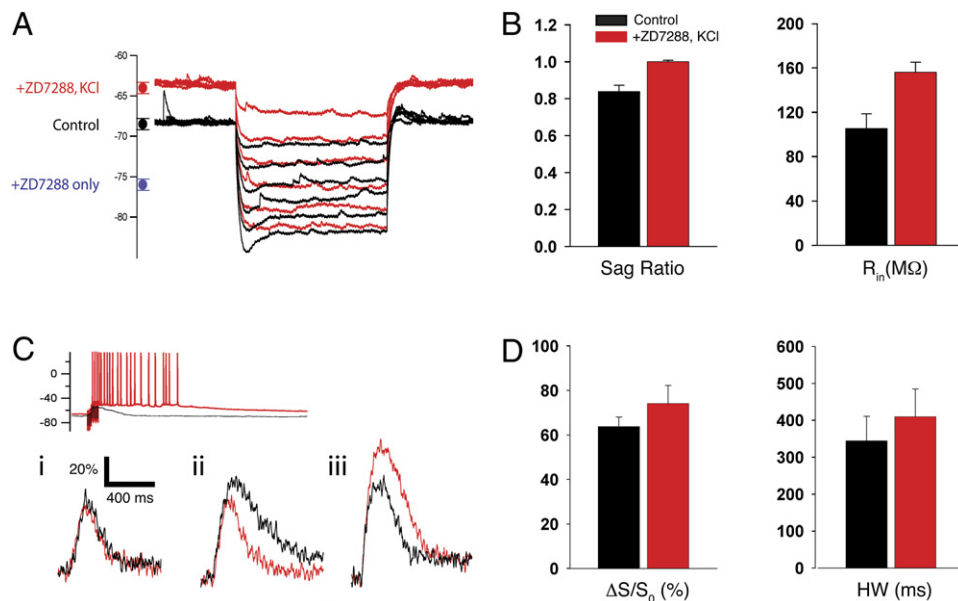


Figure 8. Coapplication of ZD7288 with Elevated KCl Prevents the Hyperpolarization Induced by I_h Blockade and Inhibits Ca²⁺ Spike Enhancement

(A) Somatic voltage responses to hyperpolarizing current injections in normal KCl (black traces, Control, 2.5 mM KCl) and after application of 10 μM ZD7288 plus 6.25 mM KCl (red traces). The circles on the left show mean (±SE) values of resting potential: Control (black), V_m = -68.2 ± 0.4 mV (n = 22); ZD7288 + 6.25 mM KCl (red), V_m = -63.6 ± 0.4 mV (n = 8); ZD7288 only (blue), V_m = -75.5 ± 0.45 mV (n = 7).

(B) Mean effect of ZD7288 plus 6.25 mM KCl on depolarizing sag (left) and input resistance (right). Input resistance (R_{in}): Control, 105.4 ± 13.2 MΩ; ZD7288 plus 6.25 mM KCl, 156.1 ± 9.1 MΩ. Sag ratio (steady-state/peak voltage response to hyperpolarizing current): Control, 0.84 ± 0.03; ZD7288 plus KCl, 1.00 ± 0.008 (p < 0.01, paired t test; n = 7).

(C) Example somatic voltage (top) and distal Ca²⁺ signals (bottom) in response to ZD7288 plus 6.25 mM KCl. Black traces, control (2.5 mM KCl without ZD7288). Red traces, in the presence of 10 μM ZD7288 plus 6.25 mM KCl. Application of ZD7288 plus elevated KCl did not alter or slightly decreased peak Ca²⁺ in 6 of 8 cells (examples i and ii). In 2 of 8 cells, ZD7288 plus elevated KCl increased the Ca²⁺ signal (iii). Increase in KCl enhanced excitability in all 8 cells, leading to prolonged firing in response to PP stimulation.

(D) Pooled data for effects of ZD7288 plus 6.25 mM KCl on mean distal Ca²⁺ signal amplitude (ΔS/S₀) and duration (HW). Control: ΔS/S₀ = 66.4% ± 5.8%, HW = 344.6 ± 66.3 ms; ZD7288 + KCl: ΔS/S₀ = 74.2% ± 8.1% (p = 0.34, n = 7), HW = 409.7 ± 75.3 ms (p = 0.27, n = 7).

synergistic actions. First, the hyperpolarization of the resting membrane removes resting inactivation of T- and N-type VGCCs, which enhances subsequent Ca²⁺ influx during a spike. Second, the increase in input resistance increases temporal integration and allows an EPSP to reach threshold to trigger a Ca²⁺ spike despite the hyperpolarization.

Counteracting the Hyperpolarization Induced by I_h Blockade Occludes the effects on Calcium Enhancement

To provide an experimental test of the importance of membrane hyperpolarization for the enhancement in the Ca²⁺ spike, we counterbalanced the normal hyperpolarization upon blockade of I_h with ZD7288 by elevating external K⁺, similar to the simulation results with an altered E_K. Distal Ca²⁺ signals were measured before and after bath application of ZD7288 (10 μM) in elevated (6.25 mM) KCl. This concentration of KCl was calculated to be appropriate for maintaining the distal dendritic resting potential at its normal level upon blockade of I_h (see Supplemental Data).

Application of ZD7288 in elevated KCl was still effective at blocking HCN channels, as evident by the block of the hyperpolarization-induced voltage sag normally caused by I_h activation (Figure 8A). Importantly, the addition of KCl to the ZD7288 solution was also effective in preventing the hyperpolarization of the somatic resting potential. Whereas application of ZD7288 alone hyperpolarized the membrane from its normal value of -68.1 ± 1.3 mV to -75.5 ± 0.45 mV, coapplication of ZD7288 plus 6.25 mM KCl resulted in a slight depolarization of the resting membrane to -63.6 ± 0.4 mV. Although the somatic membrane potential is 4–5 mV more positive than its original resting potential in 2.5 mM KCl in the absence of ZD7288, the KCl concentration of 6.25 mM is what we calculated as being necessary to maintain the resting potential of the distal dendritic membrane at its normal level upon blockade of I_h, due to its high density of I_h (see Supplemental Data).

When we delivered a burst of distal PP stimulation in the presence of ZD7288 plus 6.25 mM KCl, the normal effect of I_h blockade to prolong the distal Ca²⁺ spikes was largely eliminated (Figures 8C and 8D). In 6 out of 8 cells examined, application of ZD7288 plus KCl either had no effect

on Ca²⁺ spike duration and amplitude or caused a small decrease (Figure 8C). However, in 2 of the 8 cells, there was still a substantial increase in Ca²⁺ signal peak amplitude and duration, similar to what we observed when ZD7288 was applied alone. This may reflect variability in the distal dendritic resting potential (Kole et al., 2006). Alternatively, it may reflect a small hyperpolarization-independent component of the effect of ZD7288 plus 6.25 mM KCl, due to the increase in input resistance and decrease in K⁺ driving force, as observed in the computational model (Figure 7B). On average over all eight experiments, application of ZD7288 plus 6.25 mM KCl produced an ~12% increase in the peak Ca²⁺ signal (Control: $\Delta S/S_0 = 66.4\% \pm 5.8\%$; ZD7288 plus KCl: $\Delta S/S_0 = 74.2\% \pm 8.1\%$, $p = 0.34$) accompanied by an ~19% increase in half-width (Control: 344.6 ± 66.3 ms; ZD7288 plus KCl: 409.7 ± 75.3 ms, $p = 0.27$) (Figure 8D). These effects were significantly smaller than the 17% ($p < 0.01$) increase in peak and 57% ($p < 0.01$) increase in duration of the Ca²⁺ signals when ZD7288 was applied alone (see Figure 3). Thus, in agreement with the model, our experimental results are consistent with the view that membrane hyperpolarization makes an important contribution to the enhancement in the distal dendritic Ca²⁺ signal upon blockade of I_h.

DISCUSSION

This study describes a mechanism by which HCN channels constrain nonlinear Ca²⁺ events at distal dendrites of CA1 pyramidal neurons, providing an explanation for the widespread finding that blockade of the excitatory I_h enhances dendritic excitability. We find that the unique effects of I_h to decrease input resistance while depolarizing the resting membrane exert a powerful inhibitory influence on Ca²⁺ spikes generated in distal dendrites. As a result, reduction of I_h, either due to HCN1 deletion or pharmacological blockade, leads to an increase in the peak amplitude and a dramatic prolongation in duration of the distal Ca²⁺ signals elicited by a short burst of perforant path synaptic stimulation.

According to our pharmacological results, the distal Ca²⁺ events are triggered by synaptic activation of both AMPA and NMDA receptors, which generates an initial depolarization that then activates both Ni²⁺-insensitive T-type and N-type voltage-gated Ca²⁺ channels. Immunocytochemical studies show that the Ni²⁺-insensitive Ca_v3.3 subunit is the major T-type isoform expressed in the distal CA1 neuron dendrites (McKay et al., 2006), suggesting that this isoform participates in the distal Ca²⁺ spikes. Interestingly Ca_v3.3 channels display significantly slower inactivation kinetics than the other T-type channel isoforms (Ca_v3.1 and Ca_v3.2), with time constants of inactivation >50 ms, appropriate for generating long-lasting Ca²⁺ spikes (Lee et al., 1999). The N-type channels display even slower inactivation kinetics, with time constants > 100 ms (Fox et al., 1987; Nowycky et al., 1985). These two VGCCs also show relatively slow activation kinetics

and require relatively strong depolarizations to activate, with midpoint activation voltages of -21 mV for Ca_v3.3 (Lee et al., 1999) and +10 mV for N-type channels (Fox et al., 1987; Nowycky et al., 1985). Thus, the triggering of regenerative events mediated by such channels will require large, long depolarizations, such as those elicited by bursts of synaptic stimulation. Finally, the steady-state inactivation of both Ca_v3.3 and N-type VGCCs shows a steep dependence on voltage near typical resting membrane potentials. As a result, steady-state availability of these channels will be responsive to small changes in resting potential.

Our computational and experimental findings indicate that the voltage-dependent properties of I_h are finely tuned to interact with the voltage-dependent gating of the T- and N-type Ca²⁺ channels to regulate the distal Ca²⁺ spikes. The effect of I_h to depolarize the resting membrane increases the steady-state inactivation of these VGCCs, whereas the effect of I_h to decrease the input resistance reduces the size of the EPSP, thus decreasing the voltage-dependent activation of the calcium channels. These combined effects of I_h therefore exert a powerful inhibitory effect on T- and N-type channel opening, thus inhibiting Ca²⁺ influx during the distal dendritic Ca²⁺ spikes. As dendrites contain an array of voltage-gated channels in addition to I_h, other ionic mechanisms are also likely to regulate the distal Ca²⁺ spikes (e.g., Wei et al., 2001; Cai et al., 2004).

One surprising result from our study is that neither Ni²⁺-sensitive VGCCs (including Ca_v3.2 T-type and Ca_v2.3 R-type) nor dihydropyridine-sensitive L-type VGCCs appear to contribute to the distal Ca²⁺ spikes. These results were unexpected, as previous studies have found that either the combined application of Ni²⁺ and nimodipine (Golding et al., 2002) or the application of a high concentration of nifedipine (a dihydropyridine similar to nimodipine) alone partially inhibits perforant path LTP (Remondes and Schuman, 2003). Recently, Ni²⁺-sensitive and L-type VGCCs channels have been found to contribute to Ca²⁺ influx into CA1 neuron dendritic spines in stratum radiatum in response to local uncaging of glutamate (Bloodgood and Sabatini, 2007). Thus, the Ni²⁺-sensitive or L-type channels may participate in perforant path LTP by directly contributing to Ca²⁺ influx in spines on distal dendrites.

The inhibitory role of I_h in regulating the long-lasting Ca²⁺ spikes in CA1 dendrites in stratum lacunosum moleculare is in general agreement with previous findings that I_h inhibits other forms of dendritic excitability, such as the firing of briefer spikes in proximal CA1 dendrites in stratum radiatum (Fan et al., 2005; Magee, 1998; Poolos et al., 2002), distal dendrites in neocortical layer V neurons (Williams and Stuart, 2000; Berger et al., 2003; Kole et al., 2007), and dendrites of entorhinal cortex layer V neurons (Rosenkranz and Johnston, 2006; Shah et al., 2004). The surprisingly long duration of the Ca²⁺ spikes in the SLM dendrites that we observe is in agreement with the Ca²⁺ waveforms seen in distal CA1 dendrites of rat

hippocampal slice cultures (Wei et al., 2001; Cai et al., 2004). However, briefer Ca²⁺ spikes from distal dendrites of rat CA1 neurons have also been reported (Golding et al., 2002), suggesting that there may be different modes of regenerative activity induced by slightly different stimulus protocols. The long-lasting Ca²⁺ spikes in SLM dendrites may depend on the unique distribution of voltage-gated channels in these membranes. For example, the Kv4.2 A-type K⁺ channel, which exerts a powerful inhibitory effect on excitability, is restricted to the SR region of CA1 dendrites (Rhodes et al., 2004), where it prevents the invasion of the SR dendrites by distal Ca²⁺ spikes generated in SLM (Cai et al., 2004). Despite these differences in local ion channels, the genesis of dendritic action potentials in many neuronal cell types is often mediated by voltage-dependent Ca²⁺ channels; thus, the inhibitory mechanism that we have identified in CA1 SLM dendrites is likely to extend to other areas of the nervous system with high densities of I_h.

Recent studies have correlated the modulatory role of I_h in dendritic integration to performance in memory tasks, both for hippocampal-dependent spatial memory in mice (Nolan et al., 2004) and working memory mediated by the prefrontal cortex (Wang et al., 2007). Here we purposefully used stimulation protocols similar to those used to induce LTP at PP synapses (Golding et al., 2002; Nolan et al., 2004) to examine effects of I_h on Ca²⁺ transients that may be relevant to hippocampal memory. These distal Ca²⁺ spikes are thought to play an important role in the induction of LTP at the PP synapses, since somatic action potentials fail to backpropagate into the distal CA1 dendrites (Golding et al., 2002; Remondes and Schuman, 2003). Importantly, the peak Ca²⁺ level associated with the distal spikes can exceed 10 μM, a concentration capable of inducing LTP (Malenka et al., 1988; Yang et al., 1999). Thus, the augmentation in distal Ca²⁺ transients observed upon HCN1 deletion provides a potential mechanism for the enhancement in LTP at the PP synapses in the HCN1 KO mice. As both our study and a previous study of the role of HCN1 in LTP (Nolan et al., 2004) were performed in the presence of blockers of inhibitory synaptic transmission, it will be of interest in the future to explore the role of HCN1 when inhibition is intact.

Although the regulation of dendritic Ca²⁺ spikes that we have analyzed is due to genetic or pharmacological manipulations of I_h, HCN channels are regulated by a number of modulatory processes that are of physiological relevance. Thus, I_h is directly facilitated by the second messenger cAMP (DiFrancesco and Tortora, 1991) and the membrane lipid PI(4,5)P₂ (Pian et al., 2006; Zolles et al., 2006). Enhancement of cAMP levels by dopamine depresses dendritic excitability in entorhinal cortex neurons through a mechanism that depends on an enhancement in I_h (Rosenkranz and Johnston, 2006). Moreover, both physiological (Fan et al., 2005) and pathophysiological (Shah et al., 2004) levels of intrinsic neural activity have been found to alter levels of I_h and HCN1 expression that are associated with long-lasting changes in dendritic

integration and excitability. Conversely, a reduction in I_h, for example due to a reduction in resting levels of cAMP, may augment the distal Ca²⁺ events, potentially leading to an enhancement of LTP, as seen in the HCN1 KO mice. Thus, we suggest that the effect of I_h to constrain dendritic Ca²⁺ spikes may represent a physiologically important means for dynamically regulating dendritic integration and synaptic plasticity in a wide variety of pyramidal neurons in the central nervous system.

EXPERIMENTAL PROCEDURES

Tissue Preparation

Horizontal brain slices were prepared from P30–P50 HCN1 KO mice (–/–) or wild-type (+/+) littermates (Nolan et al., 2003). Mice were deeply anesthetized with isoflurane and their brains rapidly removed and placed in cold (2°C–3°C) modified ACSF containing (in mM) NaCl (10), NaH₂PO₄ (1.25), KCl (2.5), NaHCO₃ (25), glucose (25), CaCl₂ (0.5), MgCl₂ (7), sucrose (190), and Na-pyruvate (2), equilibrated with 95%/5% O₂/CO₂. The hemisected brain was glued to an agar block (angled 10° in the ventromedial direction for optimal preservation of SLM perforant path inputs) and cut submerged in cold ACSF into 300 μm sections with a Vibratome 1000. Slices were transferred to standard ACSF at 35°C for 30–60 min and then kept at room temperature (21°C–22°C). Experiments were performed 1.5–7 hr after slice preparation.

Electrophysiology Recordings and Solutions

The standard ACSF had the following composition (mM): NaCl (125), NaH₂PO₄ (1.25), KCl (2.5), NaHCO₃ (25), glucose (25), CaCl₂ (2), and MgCl₂ (1). In all experiments, inhibitory transmission was blocked by the GABA_A and GABA_B receptor antagonists gabazine (1 μM) and CGP-55845 (2 μM), respectively. Whole-cell recordings were obtained from CA1 pyramidal cells in submerged slices at 33°C–35°C. Neurons were visually identified using DIC optics and contrast enhancement with a digital camera (Hamamatsu). Patch pipettes (2.5–5 MΩ) were filled with intracellular solution containing (mM) KMeSO₄ (130), KCl (10), HEPEs (10), NaCl (4), MgATP (4), Na₂GTP (0.3), phosphocreatine (10), and calcium-insensitive (Alexa Fluor 594, 25 μM) and calcium-sensitive (Oregon Green BAPTA-5N, 500 μM) dyes. Series resistance was less than 20 MΩ in somatic and less than 50 MΩ in dendritic recordings; capacitance was fully compensated throughout the experiment.

Fluorescent indicators (Alexa 594 cadaverine, Fluo-4 cadaverine, Oregon-Green BAPTA-5N) were purchased from Molecular Probes (Invitrogen, Carlsbad, CA), diluted into 100× stock solutions using standard intracellular solution, aliquoted, and frozen (–20°C). Pharmacological antagonists were added to the bath solution by dilution from stock solutions (500- to 1000-fold concentrated). All drugs were obtained from either Sigma or Tocris-Cookson and used at the following concentrations (μM): CPA (30), D-APV (50), gabazine (1), CGP-55845 (2), CNQX (10), ω-conotoxin GVIA (1), mibefradil (20), and nimodipine (20).

Two-Photon Ca²⁺ Imaging

Two-photon imaging was performed using a BioRad Radiance 2100 MP (Zeiss, Jena, Germany), powered by a MaiTai Ti:sapphire pulsed laser (Spectra-Physics, Fremont, CA) tuned to 800 nm. Red (Alexa 594 cadaverine; Ca²⁺ insensitive) and green (Oregon Green BAPTA-5N or Fluo-4 cadaverine; Ca²⁺ sensitive) epifluorescent signals were collected through a 60× 1.1 NA objective (Olympus, Center Valley, PA) and measured by custom external GaAsP detectors (Multiphoton Peripherals Inc., Ithaca, NY). Optical signals were digitized through the Radiance system using Lasersharpe 2000 software (Zeiss) and analyzed offline in Igor Pro (Wavemetrics, Lake Oswego, OR). The Ca²⁺ signal (S) was defined as the ratio of the calcium-dependent green

fluorescence versus the calcium-independent red fluorescence (G/R), using low-pass filtered averages of three to five individual linescans, normalized to the prestimulus baseline (see [Supplemental Methods](#) for details).

Electrophysiological Data Acquisition and Analysis

Recordings were obtained using a two-channel Multiclamp 700B amplifier (Molecular Devices, Sunnyvale, CA). Data were digitized on a Windows PC using an ITC-18 A/D board (Instrutech Instruments, Port Washington, NY) controlled by either PULSE acquisition software (Heka Instruments) or custom routines written in Igor Pro (Wavemetrics, Eugene, OR). All current-clamp data were acquired at 20 kHz and low-pass filtered at 4 kHz using the Multiclamp 700B Bessel filter. Analysis was performed using custom routines written in Igor Pro. Statistical tests were performed using Excel (Microsoft, Redmond, WA) and SigmaStat (Systat Software, Inc., San Jose, CA).

Computational Modeling

Nonlinear, synaptically evoked regenerative events at distal dendrites were simulated in NEURON (Carnevale and Hines, 2006; available at <http://www.neuron.yale.edu/neuron>) using a single-compartment model (dendrite of 25 μm length and 1 μm diameter) with the following active channel conductances (in $\text{pS}/\mu\text{m}^2$): g_{Na} (45), $g_{\text{K,DR}}$ (4), $g_{\text{K,A}}$ (640), g_{H} (20), g_{LEAK} (10), $g_{\text{Ca,T}}$ (60), and $g_{\text{Ca,N}}$ (30). A specific capacitance of 2 $\mu\text{F}/\text{cm}^2$ was used to account for spine surface area. The I_{h} conductance value was chosen to yield a membrane potential shift of ~ 6 mV upon removal of 80% of the conductance, matching our experimental observations. Synaptic current (ten synapses, 350 pS conductance each) was simulated using custom models of AMPA and NMDA receptor kinetics ([Supplemental Data](#)).

The predicted fluorescence signal was simulated by implementing a model of Ca²⁺ binding and extrusion assuming first-order enzyme kinetics in Matlab 7 (Mathworks, Natick, MA). The model included (concentrations in μM) calbindin (40), extrusion via membrane pumps (240), a very low-affinity endogenous buffer (10,000), and OGB-5N (500). The model was constrained by varying densities of buffers and transporters to yield a Ca²⁺ fluorescence signal whose amplitude and time course matched our experimental observations. Further details of simulations with references are given in [Supplemental Data](#).

Supplemental Data

The Supplemental Data for this article can be found online at <http://www.neuron.org/cgi/content/full/56/6/1076/DC1/>.

ACKNOWLEDGMENTS

This work was partially supported by HHMI (S.A.S.), a grant from NIH (NS R01-36658 to S.A.S.), NYSTAR, the NIH MSTP (D.T.), and an NIH training grant (J.T.D.).

Received: August 15, 2007

Revised: October 8, 2007

Accepted: November 26, 2007

Published: December 19, 2007

REFERENCES

Berger, T., Senn, W., and Lüscher, H.R. (2003). Hyperpolarization-activated current I_{h} disconnects somatic and dendritic spike initiation zones in layer V pyramidal neurons. *J. Neurophysiol.* 90, 2428–2437.

Bloodgood, B.L., and Sabatini, B.L. (2007). Nonlinear regulation of unitary synaptic signals by CaV(2.3) voltage-sensitive calcium channels located in dendritic spines. *Neuron* 53, 249–260.

Cai, X., Liang, C.W., Muralidharan, S., Kao, J.P., Tang, C.M., and Thompson, S.M. (2004). Unique roles of SK and Kv4.2 potassium channels in dendritic integration. *Neuron* 44, 351–364.

Carnevale, N.T., and Hines, M.L. (2006). *The NEURON Book* (Cambridge, UK: Cambridge University Press).

Chen, C. (2004). ZD7288 inhibits postsynaptic glutamate receptor-mediated responses at hippocampal perforant path-granule cell synapses. *Eur. J. Neurosci.* 19, 643–649.

Chevalyere, V., and Castillo, P.E. (2002). Assessing the role of I_{h} channels in synaptic transmission and mossy fiber LTP. *Proc. Natl. Acad. Sci. USA* 99, 9538–9543.

Christie, B.R., Eliot, L.S., Miyakawa, H., and Johnston, D. (1995). Different Ca²⁺ channels in somata and dendrites of hippocampal pyramidal neurons mediate spike-induced Ca²⁺ influx. *J. Neurophysiol.* 73, 2553–2557.

DiFrancesco, D., and Tortora, P. (1991). Direct activation of cardiac pacemaker channels by intracellular cyclic AMP. *Nature* 351, 145–147.

Eller, P., Berjukov, S., Wanner, S., Huber, I., Hering, S., Knaus, H.G., Toth, G., Kimball, S.D., and Striessnig, J. (2000). High affinity interaction of mibefradil with voltage-gated calcium and sodium channels. *Br. J. Pharmacol.* 130, 669–677.

Fan, Y., Fricker, D., Brager, D.H., Chen, X., Lu, H.C., Chitwood, R.A., and Johnston, D. (2005). Activity-dependent decrease of excitability in rat hippocampal neurons through increases in I_{h} . *Nat. Neurosci.* 8, 1542–1551.

Felix, R., Sandoval, A., Sanchez, D., Gomora, J.C., De la Vega-Beltran, J.L., Trevino, C.L., and Darszon, A. (2003). ZD7288 inhibits low-threshold Ca(2+) channel activity and regulates sperm function. *Biochem. Biophys. Res. Commun.* 311, 187–192.

Fox, A.P., Nowycky, M.C., and Tsien, R.W. (1987). Kinetic and pharmacological properties distinguishing three types of calcium currents in chick sensory neurones. *J. Physiol.* 394, 149–172.

Gasparini, S., Migliore, M., and Magee, J.C. (2004). On the initiation and propagation of dendritic spikes in CA1 pyramidal neurons. *J. Neurosci.* 24, 11046–11056.

Golding, N.L., and Spruston, N. (1998). Dendritic sodium spikes are variable triggers of axonal action potentials in hippocampal CA1 pyramidal neurons. *Neuron* 21, 1189–1200.

Golding, N.L., Staff, N.P., and Spruston, N. (2002). Dendritic spikes as a mechanism for cooperative long-term potentiation. *Nature* 418, 326–331.

Golding, N.L., Mickus, T.J., Katz, Y., Kath, W.L., and Spruston, N. (2005). Factors mediating powerful voltage attenuation along CA1 pyramidal neuron dendrites. *J. Physiol.* 568, 69–82.

Jarsky, T., Roxin, A., Kath, W.L., and Spruston, N. (2005). Conditional dendritic spike propagation following distal synaptic activation of hippocampal CA1 pyramidal neurons. *Nat. Neurosci.* 8, 1667–1676.

Kole, M.H., Hallermann, S., and Stuart, G.J. (2006). Single I_{h} channels in pyramidal neuron dendrites: properties, distribution, and impact on action potential output. *J. Neurosci.* 26, 1677–1687.

Kole, M.H., Brauer, A.U., and Stuart, G.J. (2007). Inherited cortical HCN1 channel loss amplifies dendritic calcium electrogenesis and burst firing in a rat absence epilepsy model. *J. Physiol.* 578, 507–525.

Lee, J.H., Daud, A.N., Cribbs, L.L., Lacerda, A.E., Pereverzev, A., Klockner, U., Schneider, T., and Perez-Reyes, E. (1999). Cloning and expression of a novel member of the low voltage-activated T-type calcium channel family. *J. Neurosci.* 19, 1912–1921.

London, M., and Hausser, M. (2005). Dendritic computation. *Annu. Rev. Neurosci.* 28, 503–532.

Lorincz, A., Notomi, T., Tamas, G., Shigemoto, R., and Nusser, Z. (2002). Polarized and compartment-dependent distribution of HCN1 in pyramidal cell dendrites. *Nat. Neurosci.* 5, 1185–1193.

Magee, J.C. (1998). Dendritic hyperpolarization-activated currents modify the integrative properties of hippocampal CA1 pyramidal neurons. *J. Neurosci.* 18, 7613–7624.

- Magee, J.C. (1999). Dendritic Ih normalizes temporal summation in hippocampal CA1 neurons. *Nat. Neurosci.* *2*, 508–514.
- Magee, J.C., and Johnston, D. (2005). Plasticity of dendritic function. *Curr. Opin. Neurobiol.* *15*, 334–342.
- Malenka, R.C., Kauer, J.A., Zucker, R.S., and Nicoll, R.A. (1988). Post-synaptic calcium is sufficient for potentiation of hippocampal synaptic transmission. *Science* *242*, 81–84.
- McKay, B.E., McRory, J.E., Molineux, M.L., Hamid, J., Snutch, T.P., Zamponi, G.W., and Turner, R.W. (2006). Ca(V)3 T-type calcium channel isoforms differentially distribute to somatic and dendritic compartments in rat central neurons. *Eur. J. Neurosci.* *24*, 2581–2594.
- Mills, L.R., Niesen, C.E., So, A.P., Carlen, P.L., Spigelman, I., and Jones, O.T. (1994). N-type Ca²⁺ channels are located on somata, dendrites, and a subpopulation of dendritic spines on live hippocampal pyramidal neurons. *J. Neurosci.* *14*, 6815–6824.
- Morris, R.G., Moser, E.I., Riedel, G., Martin, S.J., Sandin, J., Day, M., and O'Carroll, C. (2003). Elements of a neurobiological theory of the hippocampus: the role of activity-dependent synaptic plasticity in memory. *Philos. Trans. R. Soc. Lond. B. Biol. Sci.* *358*, 773–786.
- Nicholson, D.A., Trana, R., Katz, Y., Kath, W.L., Spruston, N., and Geinisman, Y. (2006). Distance-dependent differences in synapse number and AMPA receptor expression in hippocampal CA1 pyramidal neurons. *Neuron* *50*, 431–442.
- Nolan, M.F., Malleret, G., Lee, K.H., Gibbs, E., Dudman, J.T., Santoro, B., Yin, D., Thompson, R.F., Siegelbaum, S.A., Kandel, E.R., et al. (2003). The hyperpolarization-activated HCN1 channel is important for motor learning and neuronal integration by cerebellar Purkinje cells. *Cell* *115*, 551–564.
- Nolan, M.F., Malleret, G., Dudman, J.T., Buhl, D.L., Santoro, B., Gibbs, E., Vronskaya, S., Buzsaki, G., Siegelbaum, S.A., Kandel, E.R., and Morozov, A. (2004). A behavioral role for dendritic integration: HCN1 channels constrain spatial memory and plasticity at inputs to distal dendrites of CA1 pyramidal neurons. *Cell* *119*, 719–732.
- Notomi, T., and Shigemoto, R. (2004). Immunohistochemical localization of Ih channel subunits, HCN1–4, in the rat brain. *J. Comp. Neurol.* *471*, 241–276.
- Nowycky, M.C., Fox, A.P., and Tsien, R.W. (1985). Three types of neuronal calcium channel with different calcium agonist sensitivity. *Nature* *316*, 440–443.
- Otmakhova, N.A., Otmakhov, N., and Lisman, J.E. (2002). Pathway-specific properties of AMPA and NMDA-mediated transmission in CA1 hippocampal pyramidal cells. *J. Neurosci.* *22*, 1199–1207.
- Pian, P., Bucchini, A., Robinson, R.B., and Siegelbaum, S.A. (2006). Regulation of gating and rundown of HCN hyperpolarization-activated channels by exogenous and endogenous PIP₂. *J. Gen. Physiol.* *128*, 593–604.
- Poolos, N.P., Migliore, M., and Johnston, D. (2002). Pharmacological upregulation of h-channels reduces the excitability of pyramidal neuron dendrites. *Nat. Neurosci.* *5*, 767–774.
- Randall, A.D., and Tsien, R.W. (1997). Contrasting biophysical and pharmacological properties of T-type and R-type calcium channels. *Neuropharmacology* *36*, 879–893.
- Remondes, M., and Schuman, E.M. (2003). Molecular mechanisms contributing to long-lasting synaptic plasticity at the temporoammonic-CA1 synapse. *Learn. Mem.* *10*, 247–252.
- Rhodes, K.J., Carroll, K.I., Sung, M.A., Doliveira, L.C., Monaghan, M.M., Burke, S.L., Strassle, B.W., Buchwalder, L., Menegola, M., Cao, J., et al. (2004). KChIPs and Kv4 alpha subunits as integral components of A-type potassium channels in mammalian brain. *J. Neurosci.* *24*, 7903–7915.
- Robinson, R.B., and Siegelbaum, S.A. (2003). Hyperpolarization-activated cation currents: from molecules to physiological function. *Annu. Rev. Physiol.* *65*, 453–480.
- Rosenkranz, J.A., and Johnston, D. (2006). Dopaminergic regulation of neuronal excitability through modulation of Ih in layer V entorhinal cortex. *J. Neurosci.* *26*, 3229–3244.
- Santoro, B., Chen, S., Luthi, A., Pavlidis, P., Shumyatsky, G.P., Tibbs, G.R., and Siegelbaum, S.A. (2000). Molecular and functional heterogeneity of hyperpolarization-activated pacemaker channels in the mouse CNS. *J. Neurosci.* *20*, 5264–5275.
- Schiller, J., Schiller, Y., Stuart, G., and Sakmann, B. (1997). Calcium action potentials restricted to distal apical dendrites of rat neocortical pyramidal neurons. *J. Physiol.* *505*, 605–616.
- Schiller, J., Major, G., Koester, H.J., and Schiller, Y. (2000). NMDA spikes in basal dendrites of cortical pyramidal neurons. *Nature* *404*, 285–289.
- Shah, M.M., Anderson, A.E., Leung, V., Lin, X., and Johnston, D. (2004). Seizure-induced plasticity of h channels in entorhinal cortical layer III pyramidal neurons. *Neuron* *44*, 495–508.
- Stuart, G., and Spruston, N. (1998). Determinants of voltage attenuation in neocortical pyramidal neuron dendrites. *J. Neurosci.* *18*, 3501–3510.
- Wang, M., Ramos, B.P., Paspalas, C.D., Shu, Y., Simen, A., Duque, A., Vijayraghavan, S., Brennan, A., Dudley, A., Nou, E., et al. (2007). alpha2A-adrenoceptors strengthen working memory networks by inhibiting cAMP-HCN channel signaling in prefrontal cortex. *Cell* *129*, 397–410.
- Wei, D.S., Mei, Y.A., Bagal, A., Kao, J.P., Thompson, S.M., and Tang, C.M. (2001). Compartmentalized and binary behavior of terminal dendrites in hippocampal pyramidal neurons. *Science* *293*, 2272–2275.
- Westenbroek, R.E., Hell, J.W., Warner, C., Dubel, S.J., Snutch, T.P., and Catterall, W.A. (1992). Biochemical properties and subcellular distribution of an N-type calcium channel alpha 1 subunit. *Neuron* *9*, 1099–1115.
- Williams, S.R., and Stuart, G.J. (2000). Site independence of EPSP time course is mediated by dendritic I(h) in neocortical pyramidal neurons. *J. Neurophysiol.* *83*, 3177–3182.
- Yang, S.N., Tang, Y.G., and Zucker, R.S. (1999). Selective induction of LTP and LTD by postsynaptic [Ca²⁺]_i elevation. *J. Neurophysiol.* *81*, 781–787.
- Zolles, G., Klocker, N., Wenzel, D., Weisser-Thomas, J., Fleischmann, B.K., Roeper, J., and Fakler, B. (2006). Pacemaking by HCN channels requires interaction with phosphoinositides. *Neuron* *52*, 1027–1036.